Ceramics International 46 (2020) 15314–15324

Contents lists available at ScienceDirect

Ceramics International

journal homepage: www.elsevier.com/locate/ceramint

# Crystallisation kinetics and structural stability of transparent $CaF_2$ glass ceramics: Dependence of light transmittance on the amount of $CaF_2$ added

Xiwang Miao[a], Xiangtao Huo[a], Lei Liu[a], Shujie Tang[a], Min Guo[a], Fangqin Cheng[b], Mei Zhang[a,b,*]

[a] State Key Laboratory of Advanced Metallurgy, School of Metallurgical and Ecological Engineering, University of Science and Technology Beijing, Beijing, 100083, PR China

[b] Institute of Resources and Environmental Engineering, Engineering Research Center of the Ministry of Education for $CO_2$ Emission Reduction and Resource Utilization, Shanxi University, Taiyuan, 030006, PR China

ARTICLE INFO

*Keywords:*
Transparent glass ceramics
$CaF_2$ nanocrystals
Crystallisation kinetics
Glass structure

ABSTRACT

The effect of $CaF_2$ addition (15.4, 20.4, 27.4 and 35.4 wt%) on the crystallisation ability and preparation of transparent glass ceramics (TGCs) containing $CaF_2$ nanocrystals was studied. It was found that samples with 15.4, 20.4, and 35.4 wt% $CaF_2$ are crystallised with multiple crystal phases, making the TGCs opaque. Only when the amount of $CaF_2$ added is increased to 27.4 wt%, TGCs with only $CaF_2$ nanocrystals can be successfully prepared by heat treatment at 630 and 730 °C for 2 h. The crystallisation activation energy of the sample with 27.4 wt% $CaF_2$ is 247.07 kJ $mol^{-1}$, and the crystallisation energy barrier to be overcome corresponds to the formation of $CaF_2$ nanocrystals rather than the formation of aluminosilicates, whose size and distribution easily make the glass opaque. Similarly, the FT-IR and XPS results indicate that as the amount of $CaF_2$ added is increased to 27.4 wt%, the polymerisation degree of the sample is more suitable for the diffusion of calcium and fluorine atoms to form only $CaF_2$ nanocrystals; therein, the corresponding mole fractions of the bridging oxygen ($O^o$), non-bridging oxygen ($O^-$), and free oxygen ($O^{2-}$) are approximately about 0.12, 0.77 and 0.11, respectively.

## 1. Introduction

Transparent glass ceramics (TGCs) are kinds of novel functional materials that simultaneously possess both crystalline and amorphous phases. Particularly, the rare earth or transition metal ion-doped optically transparent oxyfluoride glass ceramics, in which the functional nanocrystals are dispersed within the glass matrix, have attracted more attention [1–5]. Owing to their special structure, they possess not only the chemistry and mechanical stability property of the oxide glass, but also the low phonon energy and solubility characteristics of rare earth ions of the fluoride glass. Consequently they have gradually broad application prospects, particularly as optical materials in optical sensors [6–8], solid lasers [9,10], solar cell coatings [11,12], and three-dimensional displays [13,14], among others. Various oxyfluoride systems of TGCs have been discussed in the literature, such as $SiO_2$-$Al_2O_3$-$CaF_2$ [15], $SiO_2$-$Al_2O_3$-$Na_2O$-$LaF_3$ [16], $SiO_2$-$Al_2O_3$-$Na_2O$-$BaF_2$-$YF_3$ [17], $SiO_2$-$Al_2O_3$-$Na_2CO_3$-NaF-$YF_3$-$ErF_3$ [18], and $PbGeO_3$-$PbF_2$-$CdF_2$ [19]. Fluoride offers facile crystallisation characteristics; therefore, in the preparation of these TGCs, fluorides, such as $CaF_2$, $BaF_2$, $NaYF_2$, $LaF_3$, and $PbF_2$, could act as nucleating agents and crystallise early to form nanocrystals from the glass matrix through heat treatment.

The preparation of TGCs is based on the nucleation and subsequent crystallisation, in which the nanocrystal particles form and gradually grow, and are finally dispersed within the glass matrix. In order to obtain the TGCs, according to the Rayleigh scattering theory, it is imperative that the size of the formed nanocrystals be far less than visible-light wavelength and besides the refractive index of the crystal phase be closed to that of the glass matrix [3,20,21]. In other words, the optical transparency of glass ceramics is closely related to the size and concentration of formed nanocrystals. We have successfully prepared transparent $CaF_2$ glass ceramic based on the $SiO_2$-$Al_2O_3$-CaO-MgO-$CaF_2$ system and studied the relationship between the light transmission and glass crystallisation behaviour.

It's found that the size of precipitated $CaF_2$ particle is 10–25 nm and the average grain spacing is greater than 5.64 nm when the heat treatment temperature is between 630 °C and 710 °C for a period of 2 h; this meets the Rayleigh scattering condition from the quantitative point of view [22].

In the random network theory for glass structures, $CaF_2$ as nucleating agent can break the silicon-oxygen tetrahedron structure, reduce

* Corresponding author. School of Metallurgical and Ecological Engineering, University of Science and Technology Beijing, Beijing, 100083, PR China.
*E-mail address:* zhangmei@ustb.edu.cn (M. Zhang).

https://doi.org/10.1016/j.ceramint.2020.03.072
Received 21 January 2020; Received in revised form 6 March 2020; Accepted 6 March 2020
Available online 07 March 2020

the viscosity of the glass, and thus, enhance the nucleation and growth rate of crystals. Ishu Kansal [23] found that $CaF_2$ could break the silicate glass network and decrease the molar volume and glass transition temperature of oxyfluoride glasses. Mukherjee [24] found that the addition of $CaF_2$ can improve the polycrystalline crystallisation of non-transparent $SiO_2$-$Al_2O_3$-CaO glass ceramics. However, the amount of $CaF_2$ added will change the structure and viscosity to varying degrees, which may lead to different crystallisation capabilities of the parent glasses. That is, a lower amount of $CaF_2$ added may not sufficiently depolymerise the network structure enough, due to which, the viscosity of glass is relatively higher, and the energy required for atom diffusion and rearrangement is higher, thereby complicating crystallisation of only $CaF_2$ nanocrystals from the parent glasses. Conversely, a higher amount of $CaF_2$ added will increase the possibility of premature crystallisation of the $CaF_2$ and aluminosilicate phase, increase the crystal concentration, and subsequently, increase the light scattering and cause devitrification of the obtained TGCs. Hence, it is important to properly control the amount of $CaF_2$ added to ensure both crystallisation and light transmittance of the obtained TGCs. Christian Rüssel [25] prepared TGCs containing $CaF_2$ nanocrystals and studied the effect of heat treatment on the crystallisation of the parent glasses. However, the effect of the amount of $CaF_2$ added on the crystallisation of the parent glasses and the successful preparation of TGCs was not well elucidated.

In the present work, transparent $CaF_2$ glass ceramics with different amounts of $CaF_2$ were prepared. The effects of the amount of $CaF_2$ added on the crystallisation kinetics, structural changes, and phase evolution was primarily investigated. Furthermore, the microstructure and optical properties of the obtained TGCs were also analysed.

## 2. Experimental procedure

### 2.1. Sample preparation

Parent glasses with the composition of $SiO_2$-$Al_2O_3$-MgO-CaO-$CaF_2$ were synthesised by melting-quenching. The materials employed, including silicon oxide ($SiO_2$, AR), aluminium oxide ($Al_2O_3$, AR), magnesium oxide (MgO, AR), calcium carbonate ($CaCO_3$, AR), and calcium fluoride ($CaF_2$, AR) were obtained from Sinopharm Chemical Reagent Co., Ltd. The synthesised samples (TGC15.4, TGC20.4, TGC27.4, and TGC35.4) contained 15.4, 20.4, 27.4 and 35.4 wt% $CaF_2$, respectively; the specific distribution ratio is shown in Table 1. In the batch calculation, the amount of $CaF_2$ added was controlled as a variable, while the alkalinity was maintained constant.

A 100 g mixture of well mixed raw materials was placed in a tubular furnace and held for 2 h at 1500 °C, following which the melt was quickly poured into a copper mould preheated at 550 °C, and then annealed in a muffle furnace for 5 h at this temperature to obtain the parent glasses.

Approximately 20 mg of the parent glass powder was weighted for thermal analysis. Each sample was heated to 1000 °C from room temperature at the rates of 5, 10, 15, and 20 K/min, and then cooled with the furnace to room temperature under Ar atmosphere.

The obtained parent glasses were cut into pieces of dimensions 20 × 10 × 1 mm. Based on the results of the thermal analysis, the flake glasses were subjected to nucleation and crystallisation process in a muffle furnace under different heat treatment conditions. Eventually, the TGCs were prepared, both sides of which were then polished for subsequent experimental characterisation.

**Table 1**
Chemical compositions of the samples (wt%).

| Sample | $SiO_2$ | CaO | $Al_2O_3$ | MgO | $CaF_2$ |
|---|---|---|---|---|---|
| TGC15.4 | 43.90 | 7.79 | 28.69 | 4.22 | 15.40 |
| TGC20.4 | 39.67 | 7.02 | 28.69 | 4.22 | 20.40 |
| TGC27.4 | 33.76 | 6.00 | 28.69 | 4.22 | 27.40 |
| TGC35.4 | 26.92 | 4.77 | 28.69 | 4.22 | 35.40 |

### 2.2. Characterisation and measurement

Differential scanning calorimetry (DSC, STA409c, Germany) was conducted to determine the characteristic temperatures, including the glass transition temperature ($T_g$) and the crystallisation temperature ($T_c$). For this, all the samples were heated from room temperature to 1000 °C at 5–20 K/min.

The crystallisation phases of the crystallised TGCs were analysed by X-ray powder diffraction (XRD) on a TTR3 X-ray (Japan) diffractometer using a $Cu_\alpha$ irradiation source in the range of $2\theta$ = 10–90° with a scanning speed of 2°/min.

The nanocrystals of the obtained TGCs were characterised by low-voltage transmission electron microscopy (TEM, JEM-1230, Japan), conducted at an accelerating voltage of 120 kV, as well as field-emission scanning electron microscopy (FESEM, SUPRA55, Germany).

The light transmittance spectra of the parent glasses and glass ceramics were measured by an ultraviolet–visible spectrometer (Lambda 35, PerkinElmer) in the wavelength range of 190–900 nm with an internal wavelength of 1 nm.

The structural information of the glass samples was obtained through Fourier transform infrared pectroscopy (FT-IR, Nicolet iS50, USA) with the transmittance spectra recorded in the range of 4000–400 $cm^{-1}$. X-ray photoelectron spectroscopy (XPS, AXISULTRA-DLD, Japan) was also performed to analyse the chemical bonding states.

## 3. Results and discussion

### 3.1. Preparation and characterisation of the parent glasses

The parent glasses were obtained by conventional high-temperature melting. Fig. 1(a) and (b) show the phase and light transmittance of the obtained glass samples, respectively. It is clear that the TGC15.4, TGC20.4, and TGC27.4 are amorphous and visually, colourless and transparent. The transmittance in the visible range (380–780 nm) is approximately 85%, and change little with increasing the amount of $CaF_2$ from 15.4 to 27.4 wt%. However, for TGC35.4, the parent glass is partially crystallised and becomes opaque, and the crystal phases are $CaF_2$ and $CaAl_2Si_2O_8$. Therefore, when the amount of $CaF_2$ is increased to 35.4 wt%, TGCs are not produced.

To further analyse TGC15.4, TGC20.4, and TGC27.4 under different heat treatment conditions, DSC was conducted at a heating rate of 10 K/min and the results are shown in Fig. 2. The specific glass transition temperature ($T_g$) and crystallisation temperature ($T_p$) of the three glass samples are 691.0 °C, 658.1 °C, 634.8 °C and 823.1 °C, 810.4 °C 802.0 °C, respectively. Clearly, TGC15.4 has the highest $T_g$ and $T_p$, followed by TGC20.4, and TGC27.4.

Typically, the nucleation temperature of glass is approximately 10 °C higher than the glass transition temperature [26], therefore, in order to obtain transparent $CaF_2$ glass ceramics and the corresponding heat treatment temperature interval, the following heat treatments for TGC15.4, TGC20.4, and TGC27.4 were separately performed between 630 and 740 °C, 650 and 740 °C, and 680 and 760 °C, respectively.

### 3.2. Preparation and characterisation of the obtained glass ceramics

To obtain the transparent $CaF_2$ glass ceramics, the parent glasses were heat-treated at the aforementioned temperatures. The characteristics of the as-obtained glass ceramics, as well as the effect of the amount of $CaF_2$ added on the successful preparation of the TGCs, are presented in subsequent sections.

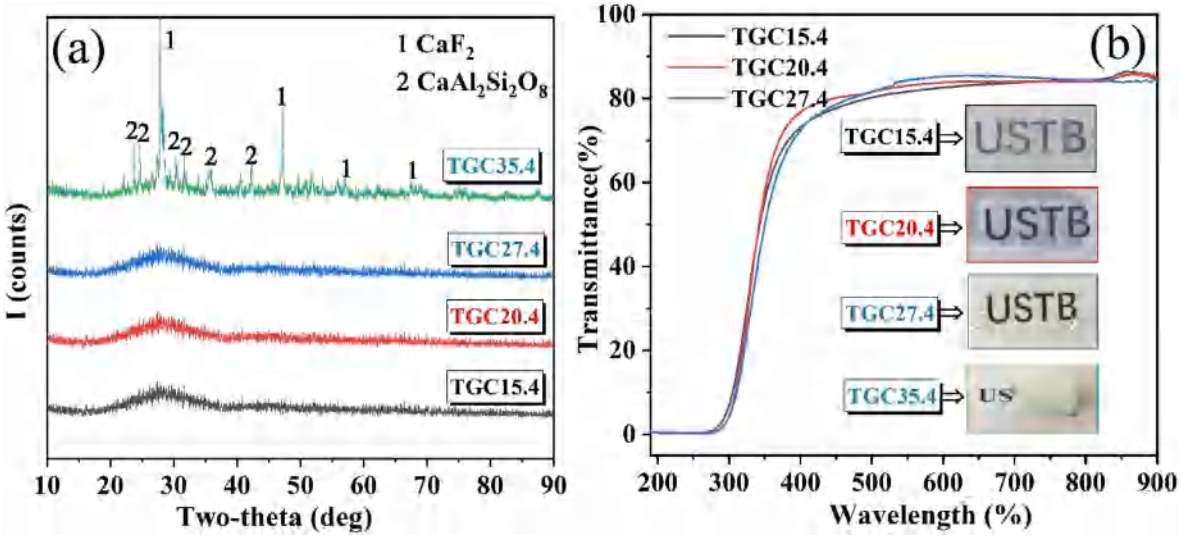


**Fig. 1.** (a)The XRD pattern and (b) Light transmittance of the obtained parent glasses. The inserts in the (b) are the physical diagrams of parent glass samples.

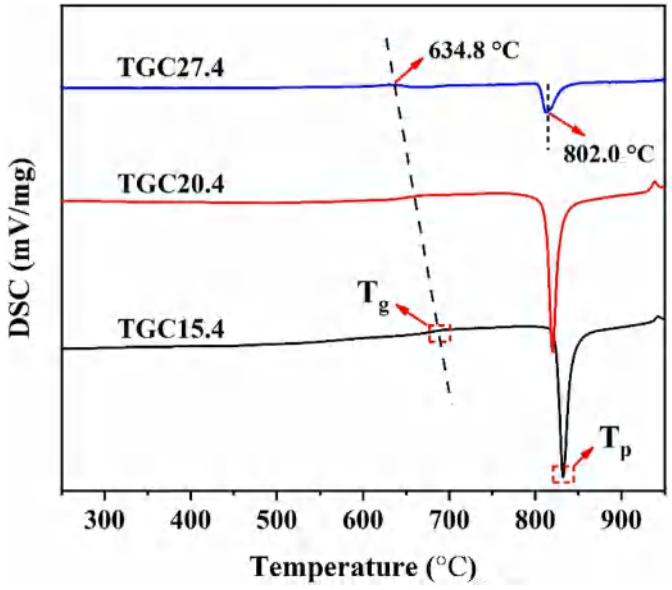


**Fig. 2.** The DSC curves obtained for parent glasses with the heat rate of 10 K/min under the Ar atmosphere.

### 3.2.1. Phase analysis for the as-obtained glass ceramics

Fig. 3 shows the XRD patterns of the crystallised glass ceramics heat-treated at different temperatures for 2 h. Fig. 3(a) shows that for TGC15.4, no crystallisation phase is generated under heat treatment between 680 and 740 °C. When heat-treated at 760 °C, the sample undergoes partial crystallisation. To further explore the law of phase transition, the sample was directly heat-treated at 820 °C, and it can be seen that besides the fluorite ($CaF_2$) phase, crystalline phases of sellaite ($MgF_2$), calcium mica ($Al_3Ca_{0.5}Si_3O_{11}$), and anorthite ($Ca(Al_2Si_2O_8)$) are simultaneously generated. Fig. 3(b) shows that for the sample TGC20.4, there is also no crystallisation peak and only amorphous peak occurs when the sample was heat-treated between 650 and 730 °C. However, when the sample was heat-treated at 740 °C, the crystallisation phases are generated, and are the same as those for TGC15.4 heat-treated at 820 °C. Fig. 3(c) shows that for the sample TGC27.4, the crystallisation peaks, which mainly occur at 28.21°, 47.04°, and 55.65°, are attributed to the crystallisation of only the $CaF_2$ phase. As the heat treatment temperature increases from 630 to 740 °C, the amorphous peak gradually disappears and the strength of crystallisation peaks increases, indicating that increasing the heat treatment temperature could accelerate the atom diffusion rate and eventually enhance the crystallisation of $CaF_2$ nanocrystals. According to the Scherrer's equation, the calculated mean grain size of the generated $CaF_2$ nanocrystals varies from 10 to 25 nm, which is far less than the wavelength of visible light.

For TGC15.4 and TGC20.4, there was no generation of only $CaF_2$ nanocrystals phase with increased heat treatment temperature; therefore, to explore whether the generation of only $CaF_2$ nanocrystals phase is related to the heat treatment time, the samples were heat-treated for a period of 6 and 10 h. The XRD patterns in Fig. 4(a) show that the phase of TGC15.4 remains amorphous when heat-treated at 710 and 730 °C for 6 and 10 h; similar experimental results occur for TGC20.4 (Fig. 4(b)). These analysis results show that there is no direct relationship between the generation of an only $CaF_2$ phase and the heat treatment time for TGC15.4 and TGC20.4.

### 3.2.2. Light transmittance property of as-obtained glass ceramics

The light transmittance spectra for the as-obtained glass ceramics obtained at different heat treatment temperatures are shown in Fig. 5. Fig. 5(a) shows that for TGC15.4, the samples are transparent and colourless when heat-treated between 680 and 740 °C. The transmittance of the samples is approximately 85%, and decays little with increasing temperature, due to the existence of only the amorphous phase and no generation of the nanocrystals phase. The actual initial crystallisation temperature is approximately 760 °C. When heat-treated at 820 °C, the sample is completely crystallised and opaque, which is attributed to the generation of the polycrystalline phase.

Similarly, Fig. 5(b) shows that for TGC20.4, the samples are transparent and colourless when heat-treated between 650 and 730 °C, and the samples become opaque when heat-treated at 740 °C. Fig. 5(c) shows that for TGC27.4, the light transmittance in the visible range (380–780 nm) decreases as the heat treatment temperature increases; moreover, the sample begins to devitrify when heat-treated at 740 °C.

### 3.2.3. Micromorphology of as-obtained glass ceramics

Fig. 6(a) and (b) show the HRTEM images of TGC15.4 heat-treated at 720 °C and TGC20.4 heat-treated at 710 °C, respectively. It is evident that there are no lattice fringes; moreover, the selected area electron diffraction (SAED) images show the diffuse halo, indicating the existence of only the amorphous phase, which also agrees with the XRD results. The TEM image of TGC27.4 heat-treated at 710 °C is shown in Fig. 6(c). The nanocrystals (region A) are evenly distributed in the glass matrix. The crystal plane spacing d value of region A is calculated to be

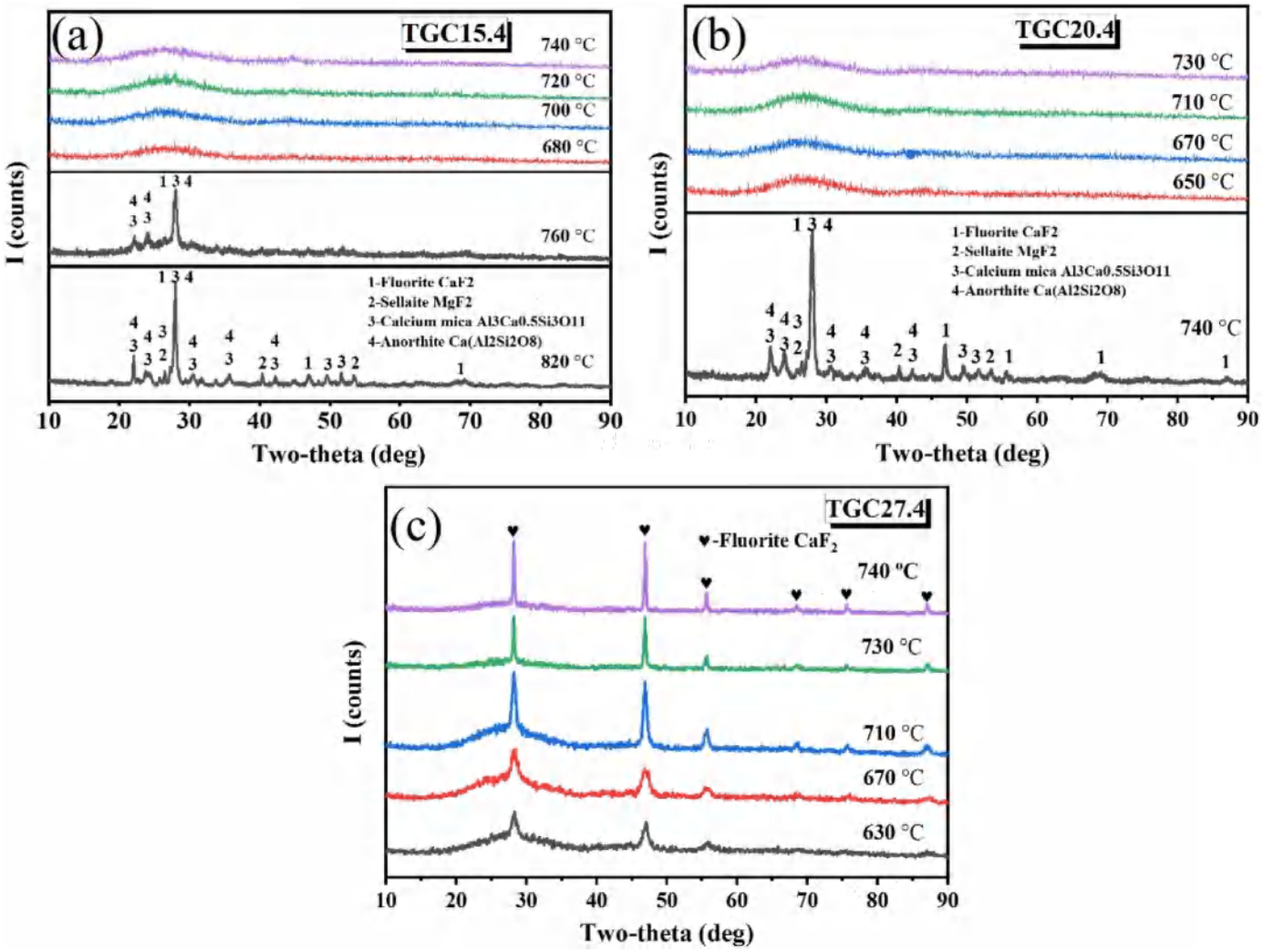


**Fig. 3.** The XRD pattern for the as-obtained glass ceramics heat-treated for a period of 2 h: (a) TGC15.4, (b) TGC20.4, (c) TGC27.4.

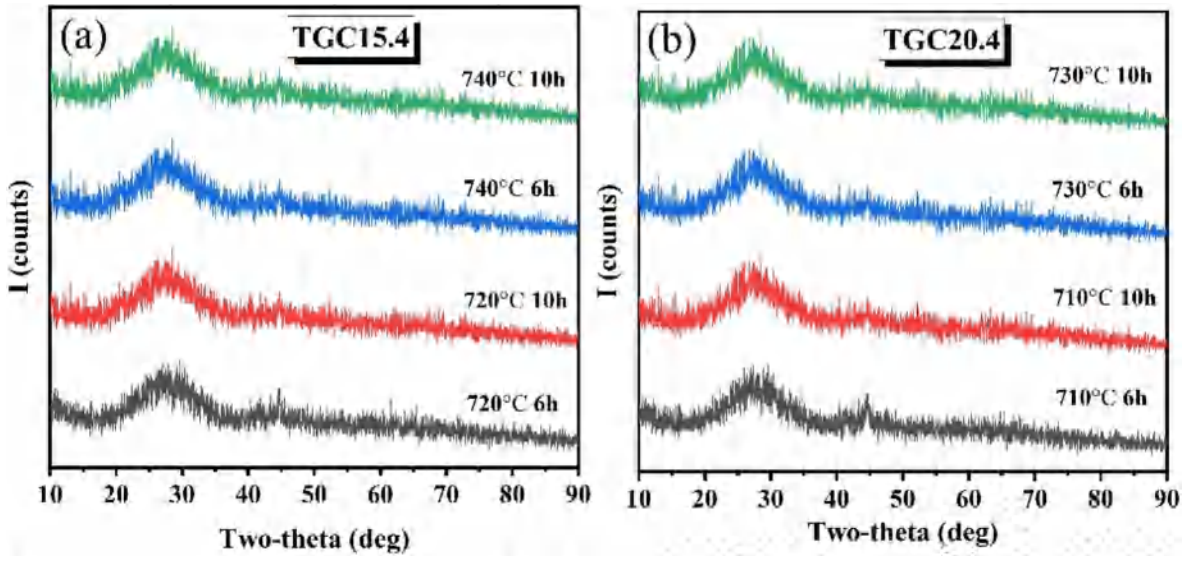


**Fig. 4.** The XRD pattern for the as-obtained glass ceramics under different heat treatment condition: (a) TGC15.4, (b) TGC20.4.

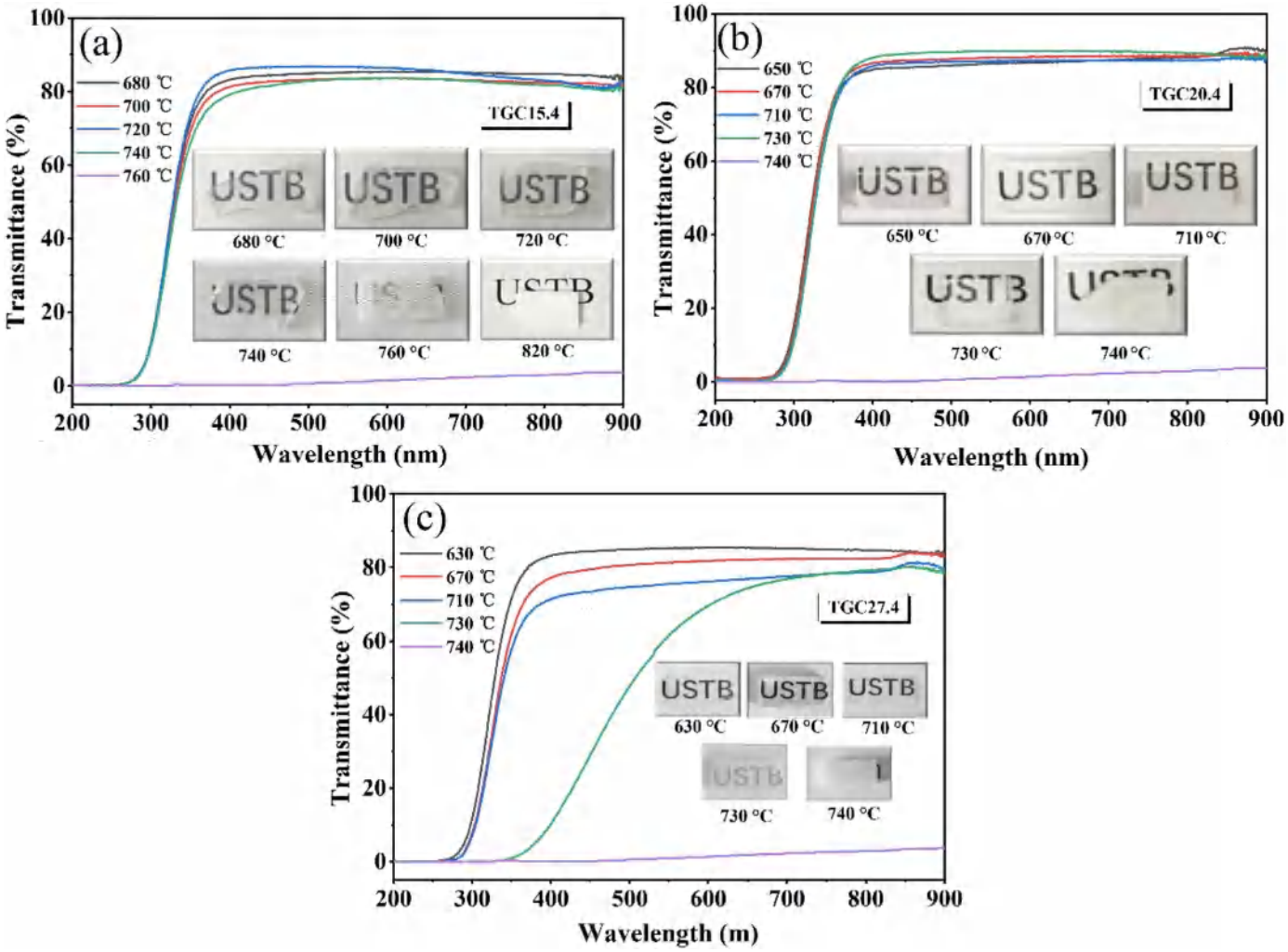


**Fig. 5.** The light transmittance curve for the as-obtained glass ceramics heat-treated for 2 h: (a) TGC15.4, (b) TGC20.4, (c) TGC27.4. The inserts are the physical diagrams of the as-obtained glass samples.

0.265 nm, which corresponds to the (220) plane of $CaF_2$ crystals and also agrees with the XRD results. Fig. 6(d) shows the SEM image of TGC20.4 heat-treated at 740 ˚C. After HF etching on the surface of the sample, large-sized round crystal particles (1#) are exposed. Besides, the atomic percentage of fluorine in the crystal particles (1#) is much higher than that of the glass matrix (2#), indicating that the crystal particles are formed by multiple crystal phases besides $CaF_2$. The size of the large particles is approximately 400 nm, which is not far less than wavelength of visible light and results to the opaque of the TGCs.

Above all, characterisation of the as-obtained glass ceramics indicated that TGC15.4 and TGC 20.4 could not be prepared as TGCs; rather, they directly became opaque with the formation of polycrystalline phases such as anorthite, whose size and quantity do not meet the criteria for Rayleigh scattering. Only when the amount of $CaF_2$ added reached 27.4 wt% was the sample successfully prepared as a TGC with only $CaF_2$ nanocrystals.

### 3.3. Crystallisation kinetics analysis

The above analyses indicated that the amount of $CaF_2$ added affects the crystallisation process of the parent glasses, and thus, contributes to the transmittance of the glass ceramics. Different amounts of $CaF_2$ added may lead to differences in the glass structure and energy barriers that must be overcome during atomic rearrangement in crystallisation, ultimately resulting in different crystallisation capabilities of the samples. This could be analysed by the crystallisation kinetics method [27–30].

#### 3.3.1. Variation in glass transition and crystallisation temperature

Fig. 7 shows the DSC curve of the parent glass of sample TGC27.4 at 5, 10, 15, and 20 K $min^{-1}$. There is one maximum endothermic peak and one maximum exothermic peak, with temperatures representing $T_g$ and $T_p$, respectively. The specific values for TGC15.4, TGC20.4, TGC27.4, and TGC35.4 at different heating rates are shown in Tables 2 and 3. The variation tends of $T_g$ and $T_p$ with the heating rate are shown in Fig. 8.

The $T_g$ and $T_p$ increase with the increased heating rate; for example, for TGC27.4, they respectively change from 902.05 to 915.15 K and 1069.65–1088.45 K with an increase in the heating rate from 5 to 20 K $min^{-1}$. In the non-isothermal crystallisation transition, the change trends of $T_g$ and $T_p$ are related to the heating rate. When heat-treated at a lower rate, there is adequate time for the parent glass to transition from glass phase to crystallisation phase, eventually resulting in lower $T_g$ and $T_p$ value, smooth crystallisation peak, and lower transition rate. Conversely, when heat-treated at a higher rate, the crystallisation transition lags, resulting in higher $T_g$ and $T_p$ value, and sharp crystallisation peak.

The $T_g$ and $T_p$ increase with decreasing amounts of $CaF_2$; for example, when heated at 5 K $min^{-1}$, they respectively change from 872.45 to 960.75 K and 1051.35–1092.85 K with decreasing amounts of

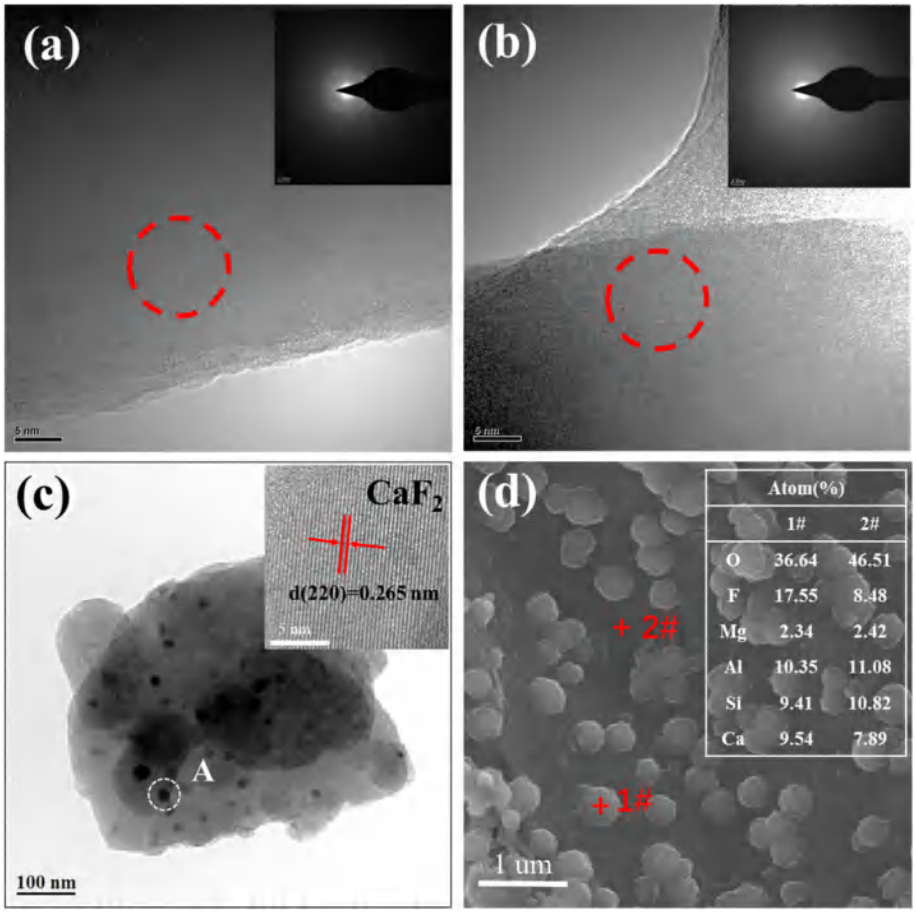


**Fig. 6.** TEM micrograph of the sample (a) TGC15.4 heat-treated at 720 °C, (b) TGC20.4 heat-treated at 710 °C, (c) TGC27.4 heat-treated at 710 °C. (d) SEM micrograph of the TGC20.4 heat-treated at 740 °C. The inset shown in (a) and (b) is the selected area electron diffraction (SAED) image. The inset shown in (c) is a high-resolution transmission electron microscope (HRTEM) image.

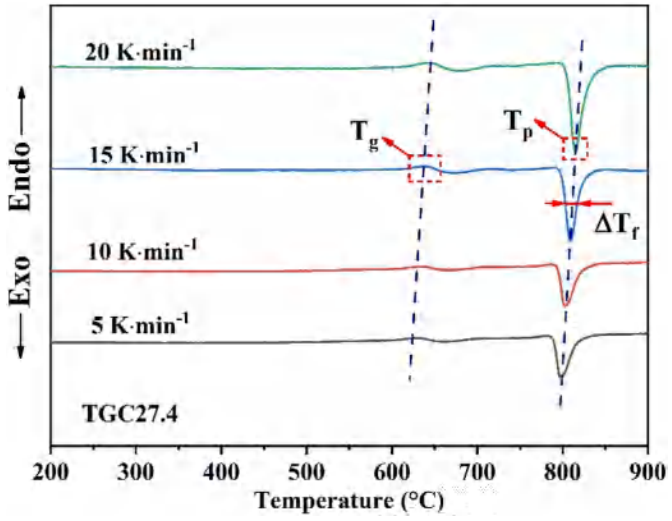


**Fig. 7.** DSC curve of the parent glass of TGC27.4 at different heating rate.

**Table 2**
Glass transition temperature ($T_g$) of samples at different heating rate.

| Heating rate (K·min$^{-1}$) | $T_g$ (K) | | | |
|---|---|---|---|---|
| | TGC15.4 | TGC20.4 | TGC27.4 | TGC35.4 |
| 5 | 960.75 | 924.35 | 902.05 | 872.45 |
| 10 | 964.15 | 931.25 | 907.95 | 881.75 |
| 15 | 967.45 | 938.65 | 910.45 | 887.35 |
| 20 | 970.35 | 945.55 | 915.15 | 890.25 |

**Table 3**
Glass crystallisation temperature ($T_p$) of samples at different heating rate.

| Heating rate (K/min) | $T_p$ (K) | | | |
|---|---|---|---|---|
| | TGC15.4 | TGC20.4 | TGC27.4 | TGC35.4 |
| 5 | 1092.85 | 1078.55 | 1069.65 | 1051.35 |
| 10 | 1096.25 | 1083.55 | 1075.15 | 1068.65 |
| 15 | 1099.75 | 1086.95 | 1081.75 | 1076.35 |
| 20 | 1106.45 | 1094.75 | 1088.45 | 1080.75 |

$CaF_2$ from 35.4 to 15.4 wt%. $CaF_2$, acting as the glass flux, could break the glass network structure to reduce the glass viscosity, and improve the crystallisation process. Hence, with an increase in the amount of added $CaF_2$ from 15.4 to 35.4 wt%, the samples exhibited decreased $T_g$ and $T_p$, and are easier to crystallise, which corresponds to the XRD results.

### 3.3.2. Crystallisation activation energy

According to the principle of crystallisation kinetics, it is found that the activation energy for crystal growth is directly related to the crystal growth rate. Based on the above thermodynamics analysis, the effects of the amount of $CaF_2$ added on the crystallisation ability of the parent glasses were further analysed by the crystallisation activation energy. Under non-isothermal conditions, the crystallisation kinetics can be analysed by the Kissinger equation [28]:

$$\ln(T_p^2/\beta) = E_a/RT_P + C \quad (1)$$

where $E_a$ (kJ·mol$^{-1}$) is the crystallisation activation energy, β (K·min$^{-1}$) is the heating rate, $T_p$ (K) represents the maximum crystallisation peak temperature value, R (8.314 J/(mol K)) is the gas

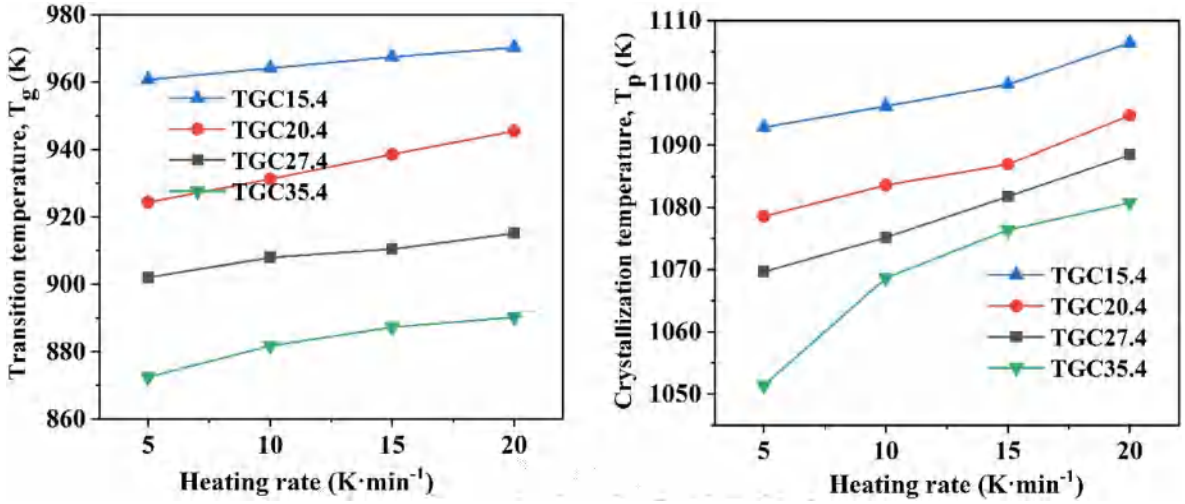


**Fig. 8.** (a) Glass transition temperature, Tg and (b) Glass crystallisation temperature, Tp as a function of heating rate of TGC15.4, TGC20.4, TGC27.4, and TGC35.4.

constant, and C is a constant. According to Eq. (1), a plot of ln ($T_P^2/\beta$) versus $1/T_p$ yields discrete points and a linear fitting curve (Fig. 9). Hence, the $E_a$ could be calculated by the slope of the fitting straight line.

The calculated $E_a$ values of TGC15.4, TGC20.4, TGC27.4, and TGC35.4 are 512.39, 337.45, 247.07 and 152.94 kJ mol$^{-1}$, respectively. It is known that the crystalline materials are more stable and have lower energy than glass body, but do not undergo transition from the transition from glass state to crystal state spontaneously. To enable this, sufficient activation energy needs to be consumed to overcome the barrier when the structural units are rearranged. It is generally believed that in the crystallisation process, the higher the crystallisation barrier, the higher is the relative activation energy required, and the lower is the crystallisation ability of the parent glasses.

TGC35.4 has the lowest activation energy, and hence, easily crystallises; the crystals precipitate directly when forming the parent glass, even without subsequent heat treatment. TGC20.4 and TGC15.4 have relatively higher activation energies; therefore, they need to overcome a higher energy barrier at a higher heat treatment temperature, resulting in the simultaneous formation of $CaF_2$ and the aluminosilicate phase, and thus making the glass ceramics opaque. Only when the amount of $CaF_2$ added is increased to 27.4 wt%, the crystallisation energy barrier of the sample to be overcome corresponds to the formation of $CaF_2$ nanocrystals rather than the formation of the aluminosilicate phase, thereby signifying the successful preparation of TGCs.

### 3.3.3. *Crystallisation mechanism analysis*

At present, there are two crystallisation mechanisms occurred to the parent glasses, namely, surface crystallisation and volume crystallisation. When the crystallisation ability of the parent glasses is very strong, the crystallisation occurs simultaneously on the surface and inside of the parent glasses, following which volume crystallisation

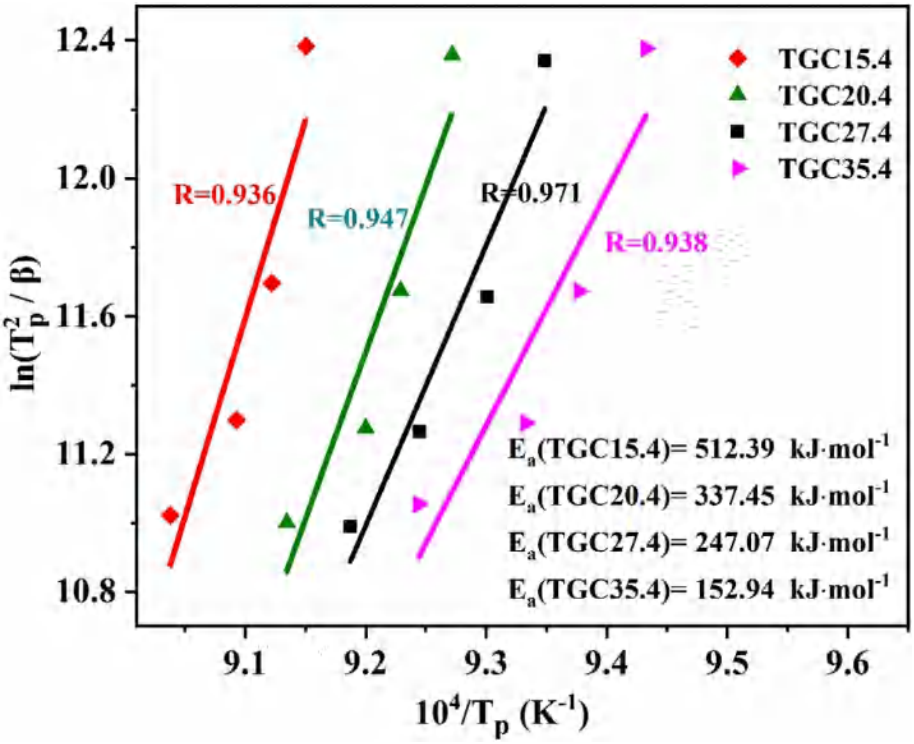


**Fig. 9.** The plot of ln($T_P^2/\beta$) versus $1/T_p$. R is the Pearson correlation coefficient. Lines represent linear fitting curves.

**Table 4**
FWHM of exothermic peak ($\triangle T_f$) of samples at different heating rate.

| Heating rate (K/min) | $\triangle T_f$ (K) | | | |
|---|---|---|---|---|
| | TGC15.4 | TGC20.4 | TGC27.4 | TGC35.4 |
| 5 | 20.51 | 17.34 | 16.26 | 15.37 |
| 10 | 18.26 | 16.54 | 16.01 | 14.92 |
| 15 | 18.34 | 16.48 | 14.23 | 13.62 |
| 20 | 16.375 | 15.02 | 13.98 | 12.37 |

**Table 5**
Crystallisation index (n) of samples at different heating rate.

| Heating rate (K/min) | n | | | |
|---|---|---|---|---|
| | TGC15.4 | TGC20.4 | TGC27.4 | TGC35.4 |
| 5 | 2.83 | 3.50 | 4.96 | 5.39 |
| 10 | 3.13 | 3.70 | 5.09 | 6.05 |
| 15 | 3.14 | 3.74 | 5.81 | 5.96 |
| 20 | 3.48 | 4.16 | 5.98 | 6.38 |

occurs; in contrast, when the crystallisation ability of the parent glass is weak, only the surface crystallisation occurs. The Avrami parameter, n, can be used to express the crystallisation mechanism of the parent glass. Typically, the higher the n value, the easier is crystallisation. When the n value exceeds 3, the parent glasses mainly crystallise by volume crystallisation, whereas when the n value is less than 3, the parent glasses mainly crystallise by surface crystallisation.

From the values of Ea and $\triangle T_f$ (shown in Table 4), n can be calculated by the Augis-Bennett equation [28]:

$$n = \frac{2.5T_p^2}{\Delta T_f E_a / R} \tag{2}$$

where $T_p$ (K) is the maximum exothermic temperature (Table 3), $E_a$ ($kJ{\cdot}mol^{-1}$) is the crystallisation activation energy, R (8.314 J/(mol K)) is the gas constant, and $\triangle T_f$ (K) is the FWHM of the exothermic peak.

The calculated n values of samples at different heating rates are shown in Table 5. It is clear that the n value increases as the amount of $CaF_2$ added increases at the same heating rate, and also increases as the heating rate increases with the same amount of $CaF_2$. Almost all n values are greater than 3, except that of TGC15.4 at 5 K/min. According to the crystallisation mechanism, the growth and crystallisation of sample TGC15.4, TGC20.4, TGC27.4, and TGC35.4 should all occur via three-dimensional interfacial volume crystallisation.

### 3.4. Structural analysis of the parent glasses

The above phase and crystallisation kinetics analyses indicate that different amounts of $CaF_2$ have a significant influence on the preparation of TGCs and the activation energy required for crystallisation; this is also reflected by the change in glass structure. The dependence of the amount of $CaF_2$ added on the glass structure is discussed with FT-IR and XPS results.

#### 3.4.1. FT-IR spectra analysis

FT-IR spectra of the glass samples extended from 1800 to 400 $cm^{-1}$ are presented in Fig. 10. The absorption band at 1520 $cm^{-1}$ is attributed to the deformation mode of H-O-H arising from molecular water within the samples or the stretching vibration of the surface O-H group [31]. The presence of the [SiO4] tetrahedron indicates a network structure of glass, and the broadened absorption band placed in the range of 1150 to 800 $cm^{-1}$ is attributed to the stretching vibration of the Si-O bond of the [SiO4] tetrahedron associated with different numbers of bridging oxygen $Q^n$ (n = 0, 1, 2, or 3) [32,33]. The $Al^{3+}$ ions play the role of a glass network intermediate, and take up the non-bridging oxygen to form the [AlO4] tetrahedron [34]. Therefore, the absorption bands at 725 and 462 $cm^{-1}$ are related to the stretching vibration of the Al-O-Al bond of the [SiO4] tetrahedron and bending vibration of the Si-O-Al bond respectively [34]. The $F^-$ ions, acting as a glass network modifier, break the network structure, and replace the oxygen atoms. Therefore, the absorption peak for the stretching vibration of the Al-F bond occurs at 1320 $cm^{-1}$ [35].

In this analysis, more attention has been paid to the stretching vibration of the [SiO4] tetrahedron. On the one hand, the $SiO_2$ content in the sample TGC15.4 is relatively the highest, consequently, the strength

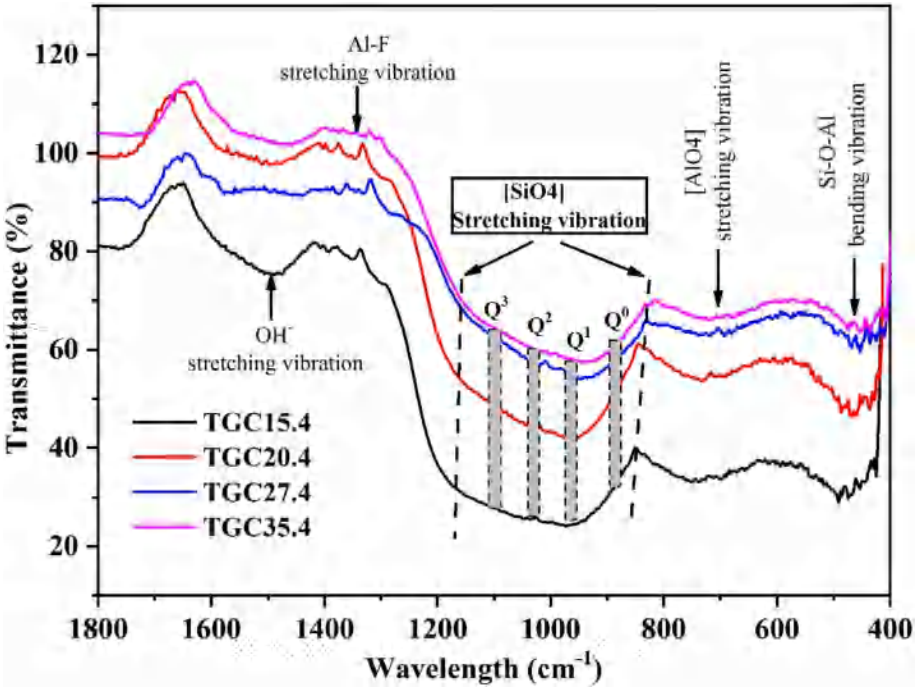


**Fig. 10.** FT-IR spectra of glass samples TGC15.4, TGC20.4, TGC27.4, and TGC35.4.

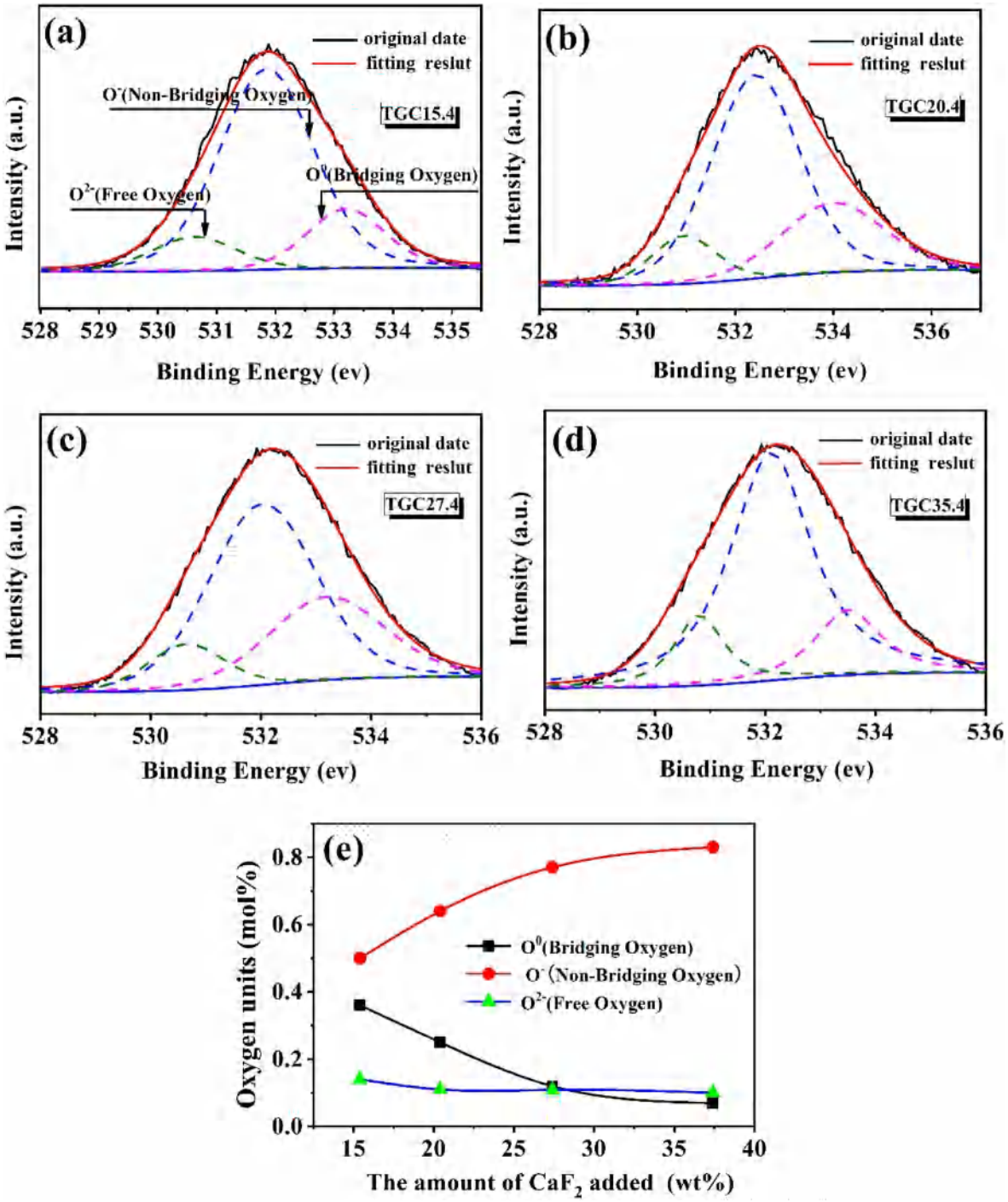


**Fig. 11.** (a)–(d) The unfolding results of $O_{1s}$ peak of TGC15.4, TGC20.4, TGC27.4, and TGC35.4, respectively. (e) The variation of the mole fraction of different oxygen atom species with the amount of $CaF_2$ added.

of the absorption band associated with the [SiO4] tetrahedron is also the highest for TGC15.4, followed by TGC20.4, TGC27.4, and TGC35.4. On the other hand, as the amount of $CaF_2$ increases to 35.4 wt%, the absorption band associated with the [SiO4] tetrahedron distinctly shifts toward a smaller wavenumber successively, indicating that the vibration energy between the [SiO4] tetrahedrons is lowered, and the degree of polymerisation of the system tends to decrease. As the amount of $CaF_2$ added is increased from 15.4 to 35.4 wt%, the bridging oxygen bonds of the samples gradually decreased and non-bridging oxygen bonds increased, leading to a transition from $Q^3$ to $Q^0$ and hence, promoting the crystallisation of the glass sample. Therefore, TGC35.4 has the strongest crystallisation tendency; this is also in agreement with the XRD results.

### 3.4.2. XPS spectra analysis

To further determine the effect of the amount of $CaF_2$ added on the variation in the mole fraction of different oxygen atom species, namely, bridging oxygen ($O^o$), non-bridging oxygen ($O^-$), and free oxygen ($O^{2-}$), the XPS measurements of the samples were conducted. Based on the Gaussian functions, the spectra of O1s peak, shown in Fig. 11(a)–(d), are deconvoluted into three peaks at approximately 534 eV, 532 eV and 531 eV, which can be ascribed to $O^o$, $O^-$, and $O^{2-}$,

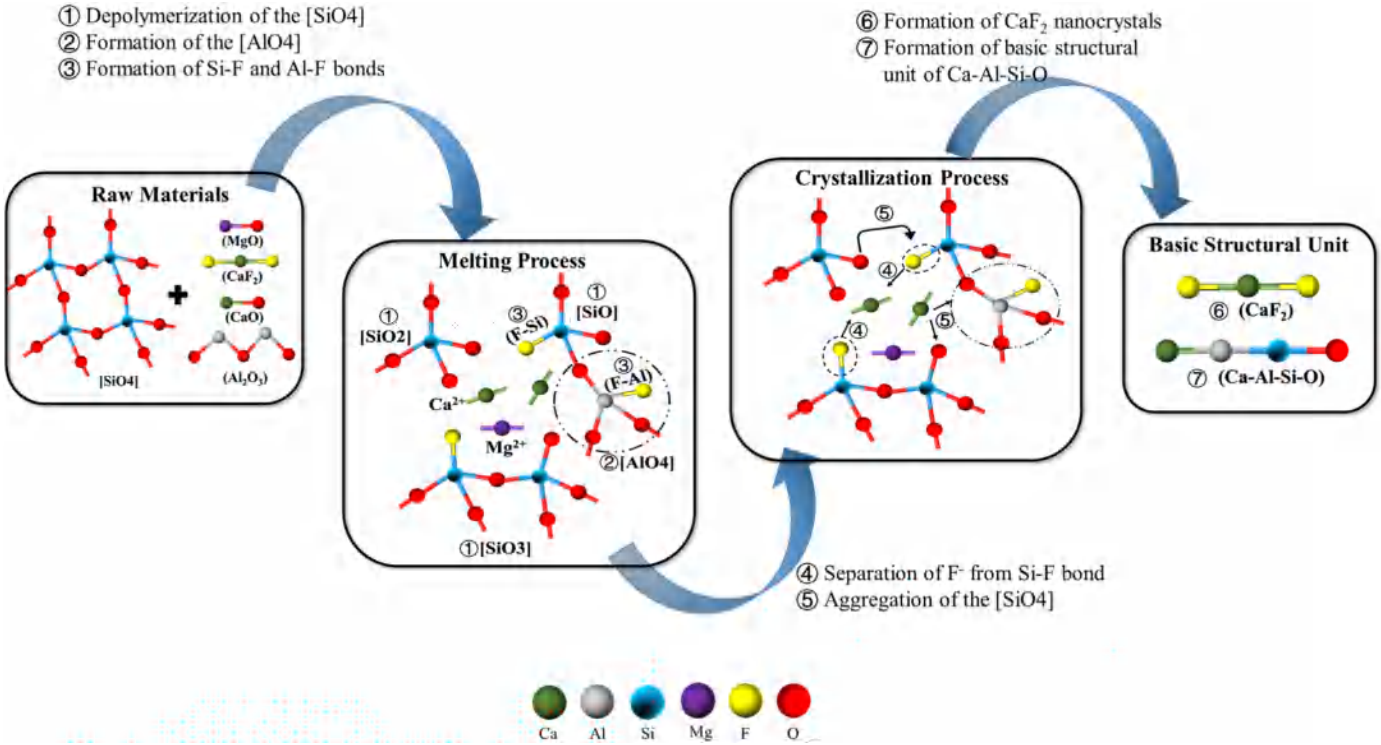


**Fig. 12.** Mechanism and model diagram of preparation process of obtained glass ceramics.

respectively [36–38]. The variation in the mole fraction of the different oxygen atom species with the amount of $CaF_2$ added is shown in Fig. 11(e). When the amount of $CaF_2$ added increases from 15.4 to 35.4 wt%, the mole fraction of the $O^-$ increases and that of $O^o$ correspondingly decreases, indicating a decrease in the polymerisation degree of the glass network structure and an enhancement in the crystallisation ability of the glass samples. There is no significant change in the mole fraction of free oxygen ($O^{2-}$). The results are the same as those of FT-IR.

A very high or very low polymerisation degree of the glass is not conducive to the preparation of the TGCs. TGC15.4 and TGC20.4 have a relatively higher polymerisation degree and a lesser crystallisation ability; hence, they cause the atoms to diffuse at a higher heat treatment temperature, eventually resulting in the formation of polycrystalline phases, and hence, making the glass ceramics opaque. Conversely, TGC35.4 has the largest mole fraction of the $O^-$ and easier atoms diffusion; therefore, polycrystalline phases are generated in the formation of the parent glass and make the glass opaque. Only when the amount of $CaF_2$ added increases to 27.4 wt%, the polymerisation degree is more suitable for the diffusion of Ca and F atoms to form the $CaF_2$ phase rather than the aluminosilicate phase at a lower heat treatment temperature, and eventually successfully prepare the TGCs containing $CaF_2$ nanocrystals; in this case, the mole fractions of $O^-$, $O^o$, and $O^{2-}$ are approximately 0.77, 0.12, and 0.11, respectively.

### 3.5. Mechanism and model of $CaF_2$ nanocrystals generation

In order to clarify the precipitation mechanism of $CaF_2$ nanocrystals, the model diagram outlining the preparation process of obtained glass ceramics is shown in Fig. 12. When melting the raw materials and obtaining the parent glass, $F^-$ ions in the $CaF_2$ can break the bridging oxygen bond of the silicon tetrahedron [SiO4] to form the Si-F bond, due to which the system contains relatively simpler structural units. $Ca^{2+}$ ions are located outside the network body, especially where the bridging oxygen bonds break, and play a role in balancing charge and accumulation. $Al_2O_3$, as the network intermediate, can take non-bridging oxygen ions to form aluminium oxide tetrahedrons [AlO4] and participate in the formation of network bodies. The Al-F bond is formed by the replacement of the $O^{2-}$ ion by $F^-$ ion. $Mg^{2+}$ ions, as network change body, are located outside the network body. During the heat treatment and crystallisation of the parent glasses, as the field of the Ca-F bond is stronger than that of the Ca-O bond, $F^-$ ions will preferentially separate from the Si-F bond and form $CaF_2$ nanocrystals with part of the $Ca^{2+}$ ions. As the heat treatment temperature continues to increase, the non-bridging oxygen will once again form the Si-O-Si bond; moreover, the accumulation of $Ca^{2+}$ ions at the broken bond increases to eventually form the Ca-Al-Si-O bonds, which are the basic structural unit of calcium mica and anorthite.

## 4. Conclusion

In this study, the TGCs with $CaF_2$ nanocrystals were prepared by the high-temperature melting, room-temperature casting, and subsequent heat treatment. The crystallisation kinetics and structure of the obtained glass ceramics were investigated in detail to determine the effect of $CaF_2$ addition on the crystallisation and preparation of TGCs with $CaF_2$ nanocrystals. When the amount of $CaF_2$ added reaches 27.4 wt%, the TGCs containing $CaF_2$ nanocrystals can be successfully prepared when heat-treated between 630 and 730 °C for 2 h; however, the samples with 15.4, 20.4, and 35.4 wt% $CaF_2$ exhibit multiple crystal phases that make the TGCs opaque. As the amounts of $CaF_2$ increases from 15.4 to 35.4 wt%, $T_g$ and $T_p$ decrease; moreover, the crystallisation activation energy decreases from 512.39 to 152.94 kJ $mol^{-1}$. Particularly, the crystallisation activation energy of the sample with 27.4 wt% $CaF_2$ is 247.07 kJ $mol^{-1}$, which just meets the energy barrier to be overcome in the formation of only $CaF_2$ crystals rather than the aluminosilicate phase whose size and distribution can easily make the glass ceramics opaque. The Avrami parameter (n) value shows that the growth and crystallisation mechanism of the samples should be three-dimensional interfacial volume crystallisation. The FT-IR and XPS results show that an increased amount of $CaF_2$ could cause the decreased polymerisation of the glass network structure, increased formation of

non-bridging bond, and stronger crystallisation ability. Compared with the polymerisation degree of the samples with 15.4, 20.4, and 35.4 wt% $CaF_2$, that of the sample with 27.4 wt% $CaF_2$ is suitable for the diffusion of calcium and fluorine atoms, which eventually form $CaF_2$ nanocrystals, thereby easily making the TGCs transparent; in this case, the mole fractions of the bridging oxygen ($O^o$), non-bridging oxygen ($O^-$), and free oxygen ($O^{2-}$) are approximately 0.12, 0.77, and 0.11, respectively.

## Declaration of competing interest

We declare that we do not have any commercial or associative interest that represents a conflict of interest in connection with the work submitted.

## Acknowledgements

The National Natural Science Foundation of China (No. U1810205, 51972019) are duly acknowledged for their financial support.

## References

[1] A. de Pablos-Martín, A. Durán, et al., Nanocrystallisation in oxyfluoride systems: mechanisms of crystallisation and photonic properties, Int. Mater. Rev. 57 (2012) 165–186.
[2] X. Liu, J. Zhou, et al., Transparent glass-ceramics functionalized by dispersed crystals, Prog. Mater. Sci. 97 (2018) 38–96.
[3] P.P. Fedorov, A.A. Luginina, et al., Transparent oxyfluoride glass ceramics, J. Fluor. Chem. 172 (2015) 22–50.
[4] M.S. Shakeri, Effect of $Y_2O_3$ on the crystallisation kinetics of $TiO_2$ nucleated LAS glass for the production of nanocrystalline transparent glass ceramics, Int. J. Min. Met. Mater. 20 (2013) 450–455.
[5] M.S. Shakeri, Fabrication, microstructure, and optical properties of nanocrystalline transparent LAST glass ceramics containing $CeO_2$, Int. J. Min. Met. Mater. 21 (2014) 401–407.
[6] M. Sobczyk, Temperature-dependent luminescence and temperature-stimulated NIR-to-VIS up-conversion in $Nd^{3+}$-doped $La_2O_3$-$Na_2O$-ZnO-$TeO_2$ glasses, J. Quant. Spectrosc. Radiat. Transfer 119 (2013) 128–136.
[7] K. Presley, J. Hwang, et al., Nanoscale upconversion for oxygen sensing, Mater. Sci. Eng. C 70 (2017) 76–84.
[8] J. Boyer, C. Carling, et al., Two-way photoswitching using one type of near-infrared light, upconverting nanoparticles, and changing only the light intensity, J. Am. Chem. Soc. 132 (2010) 15766–15772.
[9] S.B. Mirov, V.V. Fedorov, et al., Progress in mid-IR $Cr^{2+}$ and $Fe^{2+}$ doped II-VI materials and lasers, Opt. Mater. Express 1 (2011) 898–910.
[10] D.V. Martyshkin, J.T. Goldstein, et al., Crystalline $Cr^{2+}$:ZnSe/chalcogenide glass composites as active mid-IR materials, Opt. Lett. 36 (2011) 1530–1532.
[11] Z. Fang, Y. Li, et al., Enhanced sunlight excited 1-μm emission in $Cr^{3+}$-$Yb^{3+}$ co-doped transparent glass-ceramics containing $Y_3Al_5O_{12}$ nanocrystals, J. Am. Chem. Soc. 98 (2015) 1105–1110.
[12] J.C. Goldschmidt, S. Fischer, Upconversion for photovoltaics - a review of materials, devices and concepts for performance enhancement, Adv. Opt. Mater. 3 (2015) 510–535.
[13] E. Downing, L. Hesselink, et al., A three-color, solid-state, three-dimensional display, Science 5279 (1996) 1185–1189.
[14] R. Deng, F. Qin, et al., Temporal full-colour tuning through non-steady-state upconversion, Nat. Nanotechnol. 10 (2015) 237–242.
[15] G. Aldica, M. Secu, Investigations of the non-isothermal crystallisation of $CaF_2$ nanoparticles in Sm-doped oxy-fluoride glasses, J. Non-Cryst. Solids 356 (2010) 1631–1636.
[16] N. Hémono, G. Pierre, et al., Processing of transparent glass-ceramics by nanocrystallisation of $LaF_3$, J. Eur. Ceram. Soc. 29 (2009) 2915–2920.
[17] G. Krieke, A. Sarakovskis, et al., Ordering of fluorite-type phases in erbium-doped oxyfluoride glass ceramics, J. Eur. Ceram. Soc. 38 (2018) 235–243.
[18] F. Liu, E. Ma, et al., Infrared luminescence of transparent glass ceramic containing $Er^{3+}$:$NaYF_4$ nanocrystals, J. Alloys Compd. 467 (2009) 317–321.
[19] A.S. Gouveia-Neto, E.B. Da Costa, et al., Intense red upconversion emission in infrared excited holmium-doped $PbGeO_3$-$PbF_2$-$CdF_2$ transparent glass ceramic, J. Lumin. 110 (2004) 79–84.
[20] S. Hendy, Light scattering in transparent glass ceramics, Appl. Phys. Lett. 81 (2002) 1171–1173.
[21] T. Berthier, V.M. Fokin, et al., New large grain, highly crystalline, transparent glass-ceramics, J. Non-Cryst. Solids 354 (2008) 1721–1730.
[22] X. Miao, Z. Bai, et al., Controllable preparation of $CaF_2$ transparent glass ceramics: dependence of the light transmittance mechanism on the glass crystallisation behavior, Ceram. Int. 45 (2019) 8510–8517.
[23] I. Kansal, A. Goel, et al., The effect of fluoride ions on the structure and crystallisation kinetics of $La_2O_3$-containing diopside based oxyfluoride glasses, Ceram. Int. 35 (2009) 3489–3493.
[24] D.P. Mukherjee, S.K. Das, $SiO_2$-$Al_2O_3$-CaO glass-ceramics: effects of $CaF_2$ on crystallisation, microstructure and properties, Ceram. Int. 39 (2013) 571–578.
[25] C. Rüssel, Nanocrystallisation of $CaF_2$ from $Na_2O$/$K_2O$/CaO/$CaF_2$/$Al_2O_3$/$SiO_2$ glasses, Chem. Mater. 17 (2005) 5843–5847.
[26] C. Bocker, C. Rüssel, Self-organized nano-crystallisation of $BaF_2$ from $Na_2O$/$K_2O$/$BaF_2$/$Al_2O_3$/$SiO_2$ glasses, J. Eur. Ceram. Soc. 29 (2009) 1221–1225.
[27] Y. Gao, Y. Hu, et al., Effect of crystalline fraction on upconversion luminescence in $Er^{3+}$/$Yb^{3+}$ co-doped $NaYF_4$ oxyfluoride glass-ceramics, J. Eur. Ceram. Soc. 37 (2017) 763–770.
[28] Z. Bai, G. Qiu, et al., Crystallisation kinetics of glass-ceramics prepared from high-carbon ferrochromium slag, Ceram. Int. 42 (2016) 19329–19335.
[29] Z. Lu, J. Lu, et al., Effect of MgO addition on sinterability, crystallisation kinetics, and flexural strength of glass-ceramics from waste materials, Ceram. Int. 42 (2016) 3452–3459.
[30] S. Panyata, S. Eitssayeam, et al., Crystallisation kinetic of $Er^{3+}$-doped $BiO_{1.5}$-$GeO_2$-$BO_{1.5}$ glass-ceramic, Ceram. Int. 44 (2018) 46–49.
[31] Z. Wang, L. Cheng, Effect of substitution of $SiO_2$ by CaO/$CaF_2$ on structure and synthesis of transparent glass-ceramics containing $CaF_2$ nanocrystals, J. Mater. Sci. 50 (2015) 4066–4074.
[32] Z.J. Wang, Q.F. Shu, et al., Effect of $P_2O_5$ and $Fe_tO$ on the viscosity and slag structure in steelmaking slags, Metall. Mater. Trans. B 46 (2015) 758–765.
[33] J.H. Park, D.J. Min, et al., FT-IR spectroscopic study on structure of CaO-$SiO_2$ and CaO-$SiO_2$-$CaF_2$ slags, ISIJ Int. 42 (2002) 344–351.
[34] M. Rezvani, L. Farahinia, Structure and optical band gap study of transparent oxyfluoride glass-ceramics containing $CaF_2$ nanocrystals, Mater. Des. 88 (2015) 252–257.
[35] M.H. Imanieh, B.E. Yekta, et al., Crystallisation of nano calcium fluoride in $CaF_2$-$Al_2O_3$-$SiO_2$ system, Solid State Sci. 17 (2013) 76–82.
[36] M. Hayashi, N. Nabeshima, et al., Effect of fluorine on silicate network for CaO-$CaF_2$-$SiO_2$ and CaO-$CaF_2$-$SiO_2$-$FeO_x$ glasses, ISIJ Int. 42 (2002) 352–358.
[37] K.Y. Ko, J.H. Park, Effect of $CaF_2$ addition on the viscosity and structure of CaO-$SiO_2$-MnO slags, ISIJ Int. 53 (2013) 958–965.
[38] H.W. Nesbitt, G.M. Bancroft, et al., Bridging, non-bridging and free ($O^{2-}$) oxygen in $Na_2O$-$SiO_2$ glasses: an X-ray photoelectron spectroscopic (XPS) and nuclear magnetic resonance (NMR) study, J. Non-Cryst. Solids 357 (2011) 170–180.